Available online at www.sciencedirect.com

ScienceDirect

Procedia Earth and Planetary Science 9 (2014) 23 – 43

Procedia
Earth and Planetary Science

The Third Italian Workshop on Landslides

Comprehensive Instrumentation for Real Time Monitoring of Flux Boundary Conditions in Slope

Harianto Rahardjo[a,*], Alfrendo Satyanaga Nio[a], Fakhrur Rozy Harnas[a], Eng Choon Leong[a]

[a]*School of Civil and Environmental Engineering, Nanyang Technological University, 50 Nanyang Avenue Singapore 639678*

Abstract

Rainfall-induced slope failures occur in response to climatic changes in many parts of the world. Climatic changes result in dynamic flux boundary conditions across slope surface, such as infiltration and evaporation. In addition, trees, shrubs and grasses generate another dynamic process of transpiration across slope surface. As a result, stability of a slope as quantified by factor of safety is not constant over time, but varies in accordance with variation in flux boundary conditions.

Effects of flux boundary conditions on slopes can be assessed using real-time monitoring. In this paper, different types of instruments for real time monitoring of flux boundary conditions are illustrated to study the effect of rainfall and evaporation on pore-water pressure and water content in slope. Several geotechnical instruments such as piezometer, tensiometer, time-domain reflectometry and devices for measuring changes in local climate such as rainfall gauge and weather station can be installed within the slope area. The data from these instruments were captured automatically using a data acquisition system and the data were transported to a secured website in real time. Finite element seepage analyses were carried out to investigate the effect of rainwater infiltration and evaporation on pore-water pressure distribution of a residual soil slope at Telok Blangah, Singapore. The numerical analysis results showed a good agreement with those obtained from field measurements if the evaporation was applied in the analyses. This indicated that rainfall and evaporation play important roles in pore-water pressure changes within the residual soil. Seepage analyses were also conducted using different coefficients of saturated permeability and soil-water characteristic curves of the soil. The results showed that good quality laboratory test results are required to closely simulate pore-water pressure distributions within the soil layers.

Selection and peer-review under responsibility of Dipartimento di Ingegneria Civile, Design, Edilizia e Ambiente, Seconda Università di Napoli.

Keywords: Slope stability; instrumentation; infiltration; evaporation; parametric study

* Corresponding author. Tel.: +65-67905246
E-mail address: chrahardjo@ntu.edu.sg

Selection and peer-review under responsibility of Dipartimento di Ingegneria Civile, Design, Edilizia e Ambiente, Seconda Università di Napoli.
doi:10.1016/j.proeps.2014.06.015

1. Introduction

The increase of human activities in the world may accelerate the natural greenhouse effect and develop a global increase of worldwide temperatures, called global warming. As a result, many parts of the world would experience a rise of water level and significant changes in rainfall and weather patterns. Many countries in the world would encounter problems associated with slope failures. Many slope failures cause socio-economic problems. They can damage and destroy residential, commercial properties and agricultural land. Previously, researchers compiled the data of landslip fatalities in Hong Kong and drew observation that more than 470 mortalities and hundreds of public facilities were destroyed due to landslides since 1948[1]. Slope failures can be attributed to many factors, such as: rainfall, load, evaporation, temperature, slope geometry, soil properties and vegetation. However, majority of slope failures were caused by rainfall, either directly or indirectly[2,3,4,5]. In other words, slope failures pose threats to environmental sustainability.

The cost associated with slope repair is more expensive than the cost for preventive measures[6,7]. Therefore, it is important to prevent slope from failure by understanding the hydrological behavior and flux boundary condition of the slope. The flux boundary condition refers to the condition at the surface boundary that is affected by several factors, such as climate, hydrological processes, topographical features, weathering processes, human interference and vegetation[8,9,10]. Possible types of flux are infiltration, evaporation, transpiration and combinations of these three. In practice, geotechnical engineers commonly ignore flux boundary conditions at the ground surface to avoid the complexity in determining the actual flux values at the ground surface. However, in most geotechnical designs e.g. slope stability, the actual flux boundary conditions may be an important concern. Flux boundary condition produces an unsteady-state saturated/unsaturated flow situation which results in a change in the pore-water pressure and shear strength of soil[11,12]. In other words, the safety of a slope is affected by flux boundary conditions across the slope surface. Therefore, the actual flux values should be considered in geotechnical designs.

Many research works have been carried out to study the effects of climate changes (rainfall and snow), flux boundary conditions (infiltration, evaporation) and groundwater variations on slope stability through field instrumentation and numerical analyses[13,14,15,16,17,18,19,20,21,22,23,24,25,26,27,28,29,30]. Kilsby et al.[17], Rouainia et al.[18] and Mendes[19] set up BIONICS (biological and engineering impacts of climate change on slopes) project to investigate the characteristics of rainfall pattern and intensity and their effects on slope stability in United Kingdom. Glendinning et al.[20] observed that vegetative cover contributed to the reduction of rainwater infiltration and maintain the sustainability of slope infrastructure during rainfall. Springman and Teysserie[15] concluded that rainwater infiltration and snowmelt played important roles in triggering slope failures in Switzerland. Springman et al.[21] observed that the infiltration of snowmelt resulted in the rising of groundwater table which contributed to the deep seated failures in alphine moraine slopes. Johnson and Sitar[23] and Cascini et al.[24] installed several instruments on the slope to investigate the effect of groundwater flow and karst spring from the underlying bedrock on the stability of slope. Other researchers carried out seepage and stability analyses by incorporating instrumentation results from rainfall gauge, tensiometers and piezometers to investigate the effect of rainwater infiltration on slope stability. They observed that slope failures usually occurred during heavy rainfalls in Naples[25], Spain[26], Malaysia[27], Hongkong[28] and Singapore[29,30]. Previous slope stability analyses incorporating the effect of rainfall, flux boundary conditions and soil properties show that the location of critical slip surface and the occurrence of slope failure can be estimated[7,12,15,25,26,29,30]. Hence, the relevant slope preventive measures can be installed to avoid casualties and damages due to slope failures.

In this paper, different types of instruments related to real time monitoring of flux boundary conditions in slope are described. The monitoring results are incorporated in the finite element analyses to study the effect of rainfall and evaporation on pore-water pressure and water content profiles within soil layers in a residual soil slope in Singapore.

2. Slope Instrumentation

Monitoring of slope is required to observe the current condition of the slope (stability, seepage, deformation) and to evaluate the effectiveness of preventive measures. Real-time monitoring will provide the earliest possible warning whether a slope is likely to fail or preventive measures are unsuccessful. It can also be used to verify the results of

numerical analyses using finite element method. The collected data will also determine whether a single high value of measurement at a particular time is within a normal range for the instrumented slope.

Many slope failures occur due to extreme increases of pore-water pressures in the slope. Therefore, tensiometers and piezometers are required to monitor the changes of negative pore-water pressure in the unsaturated zone and the rising of ground water level inside the slope. Long term real-time monitoring is needed since rain falls throughout the entire year. The intensity of rainfall that falls on the slope is normally monitored using a tipping-bucket rain gauge. The effect of evaporation on pore-water pressures can be analyzed by monitoring the weather condition near the investigated slope, such as: temperature, net radiation, wind speed and relative humidity. The potential and actual evaporation can be calculated by incorporating the air and the soil temperatures, respectively, in the analyses using Penman's equation[31,32].

The on-line monitoring system records data in real time and the data can be accessed from any personal computer (PC) with internet connection. The on-line monitoring system can also provide trigger for actions to be taken without delay before slope failure occurs. Fig. 1 shows the schematic diagram for an on-line monitoring system. Fig. 2 shows the breakdown of instrumentation cost for an on-line monitoring system used for slope instrumentation projects in Singapore.

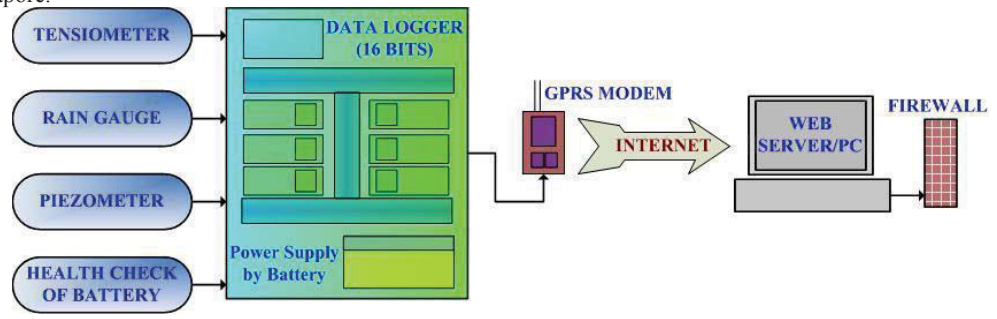

Fig. 1. Schematic diagram of instrumentation for on-line monitoring system.

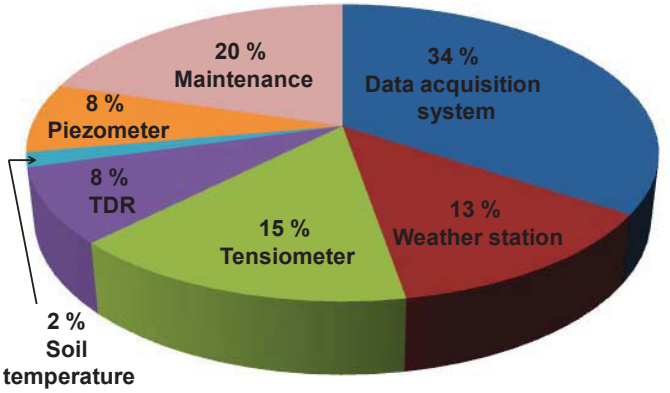

Fig. 2. General cost of a comprehensive instrumentation for on-line monitoring system in Singapore[33].

Surveying works and site investigation are usually performed prior to installation of instruments. Generally, each slope consists of 2 rows of tensiometers and 2 rows of time-domain reflectometry (TDR) distributed uniformly along the slope. Both tensiometers and TDR are installed at shallow depths of 0.5 m, 1.0 m, 1.5 m and 2.0 m. Each slope usually has three piezometers and three temperature sensors. They are installed near the crest, at midslope and near

the toe of the slope. One rain gauge is usually installed at the middle of the slope to obtain intensity of rain that falls on the slope. One weather station is installed at the top of the slope to measure air temperature, relative humidity, wind speed and net radiation. All instruments are connected to the data logger to obtain pore-water pressure, evaporation and rainfall readings. The data loggers are powered by solar panel and battery to obtain the instrumentation readings in real time. For on-line monitoring, the data logger sends all data to the server (PC) using general packet radio service (GPRS) system. GPRS sends the data using a modem installed with the data logger. The modem is connected based on internet protocols. A typical layout of instrumentation for the on-line monitoring system is shown in Fig. 3. Previous studies by several researchers[14,30,32] indicated that the monitoring data from typical numbers of instruments as illustrated in Fig. 3 are sufficient to represent the characteristics and hydrological behavior of residual soil slopes in Singapore. In addition, the maximum width, length and inclination of the instrumented area typically around 10 m, 30 m and 33°, respectively. These typical dimensions of instrumented area and the typical instruments were used to generate the typical cost for a comprehensive on-line monitoring system in Singapore as shown in Fig. 2.

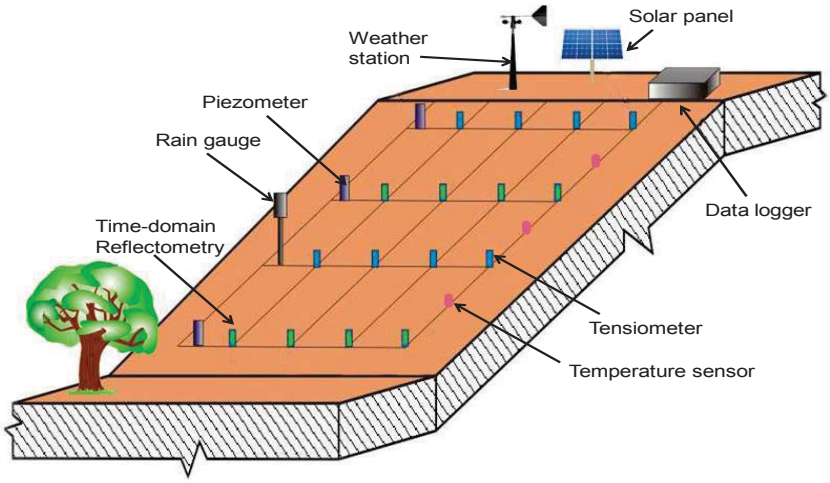

Fig. 3. Layout of instrumentation for on-line monitoring system.

All instruments must be calibrated and installed properly in order to obtain accurate readings of pore-water pressures and water content changes with respect to climatic changes within the investigated slope. The response of tensiometer must be checked prior to installation to confirm the quality and physical performance of the ceramic tip. The tensiometer holes are cored using a special hollow pipe in order to allow for a snug fit between the tensiometer tip and the soil. A layer of bentonite and a rubber pad are placed around the entrance of the tensiometer hole to seal the gap between the wall of the hole and the tensiometer body to prevent leakage of any surface water down along the tensiometer body and reaching the tensiometer tip directly. Regular maintenance of tensiometers is required to remove the accumulated air in the tensiometer tube. The accumulation of air is a result of air diffusion through the ceramic tip or cavitation of water inside the tensiometer tube.

Casagrande piezometers are commonly used for groundwater table monitoring in slope because they consist of economical components, simple to read and have long-term reliability. The piezometer tip must be placed between two bentonite layers to isolate measurements of the pore-water pressure at the tip. A low permeability layer of grout (mixture between sand and bentonite) is placed into the zone above the bentonite seal in order to prevent water migration through the zone into the intake area of the piezometer. The piezometers are fitted with depth transmitters to allow for automated data acquisition. A tipping bucket rainfall gauge is used to collect the rainfall data which must be installed in an open area and is located at 0.3 m to 1 m above the ground[34]. Regular maintenance of the rain

gauge is required as dust and insects may enter the tipping bucket and affect the accuracy of measurement of rainfall intensity.

All instruments must be installed in such a manner to minimize changes to the appearance of the original slope. All transducers from tensiometers, piezometers, rain gauge and weather station are connected to a data logger via cables. Cable protection is needed to prevent water from rainfall or ground surface leaking into the cable and damaging the circuit. All cables are arranged properly and buried inside the ground. Besides the rain gauge and the protection boxes for the instruments, the presence of instrumentation should be concealed as much as possible from public view.

The measurement of negative pore-water pressures, positive pore-water pressures and soil water content at a specific time interval are performed using tensiometers, piezometer transducers and TDR, respectively. Rainfall is frequently used as the criterion for setting the time interval for pressure reading. For example, before rainfall, the logger records readings at a 30 minutes interval. When rainfall starts, the logger will change automatically to record data every 10 minutes. The logger will still record data every 10 minutes until 30 minutes after rainfall stops. The raw data sent to the PC server must be able to be retrieved every time the user accesses the on-line monitoring website.

The data from the website will be used as an input in seepage and slope stability analyses. Based on the pore-water pressure distribution, water content profiles and the factor of safety from the numerical analyses, alert and alarm levels can be set up. The server will send the alert and alarm levels to staff in charge of the project using short message system (SMS). The system will automatically send the alert and alarm levels if the reading of the instruments exceeds the critical values. The alert and alarm levels are based on values of pore-water pressure, water content and rainfall intensity from tensiometer, piezometer and rain gauge readings. The alert level signals the staff to go to the site and check the condition of the slope. The result of the observation can be used to determine whether preventive measures should be performed to protect the slope from impending failure. The alarm level signals the staff to take action to mitigate the slope stability problem.

3. Rainfall and evaporation characteristics in Singapore

Climate in Singapore is characterized by uniform temperature and pressure, high humidity and particularly, abundant rainfalls. Based on National Environmental Agency of Singapore data, the climatic condition in Singapore is divided into two main seasons, the wetter Northeast Monsoon season from December to May and the drier Southwest Monsoon season from June to November. Maximum rainfall is usually observed between December and January, whereas June is noted as the driest month[35]. National Environmental agency of Singapore compiled the climatic data from 1981 to 2010 to produce the typical monthly rainfall, air temperature, relative humidity and wind speed in Singapore as shown in Fig. 4 to Fig. 7.

Fig. 4 indicates that the highest monthly rainfall in Singapore can be observed during the rainy period in December and January whereas the lowest monthly rainfall can be observed during the dry period in June. The typical mean monthly rainfall in Singapore is around 200 mm or 6.33 mm/day. Fig. 5 shows that the air temperature in Singapore is quite uniform throughout the year. Typical maximum, mean and minimum temperatures in a particular month are 31, 27 and 24 °C, respectively. The relative humidity in Singapore plays an important role in the calculation of potential evaporation. Fig. 6 shows that the typical maximum relative humidity is 95% and the typical minimum relative humidity can be as low as 60%. Fig. 7 shows that the wind speed in Singapore can be as high as 2.5 m/s and as low as 1.3 m/s.

The actual evaporation near the ground surface depends on soil temperature and soil suction[34]. Therefore, it is important to measure the variation of soil temperature and pore-water pressure near ground surface. Rahardjo et. al.[32] carried out analyses on the instrumented residual soil slopes from Bukit Timah Granite at Yishun (Fig. 11) in Singapore. The instrumentation readings for air and soil temperatures near ground surface for the slope at Yishun are shown in Fig. 8. The difference between air temperature and soil temperature near ground surface is plotted in Fig. 9a. Fig. 9b shows that typical maximum and minimum differences between air and soil temperatures in a given day are 3.4 °C and 0.6 °C, respectively. The maximum and minimum differences between air and soil temperatures were observed at noon (12.00 pm) and midnight (12.00 am), respectively. Since daily temperature is quite uniform for all locations in Singapore, Fig. 9b can be used to calculate soil temperature at other locations using the recorded air

temperature from NEA meteorological stations. The typical climatic data of Singapore from NEA database during the period of 1981 to 2010 were used to calculate the potential evaporation in Singapore (Fig. 10) using Penman's equation[37]. The typical minimum, mean and maximum monthly potential evaporations in Singapore are 5, 6 and 7 mm/day, respectively.

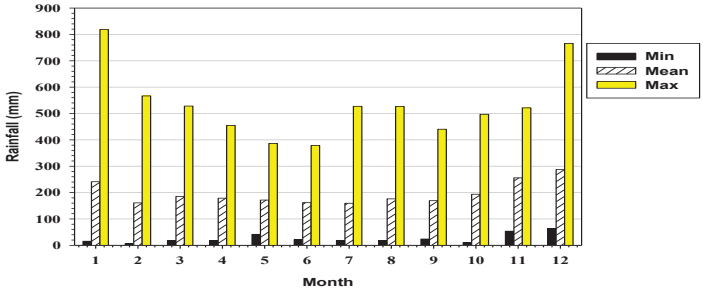

Fig. 4. Typical monthly rainfall in Singapore.

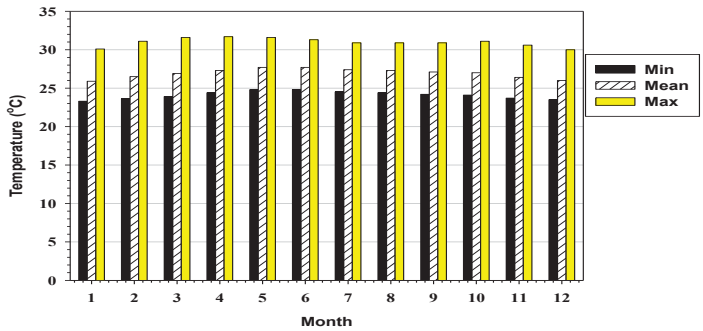

Fig. 5. Typical monthly temperature in Singapore.

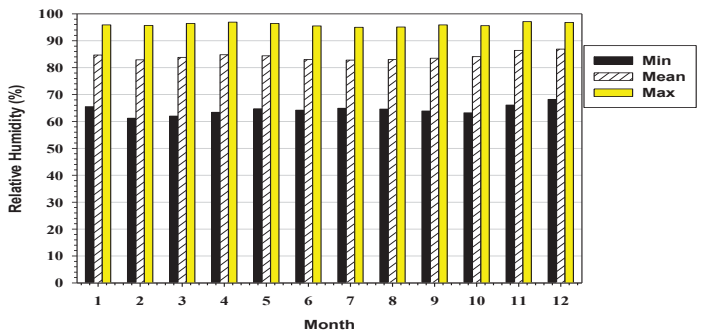

Fig. 6. Typical monthly relative humidity in Singapore.

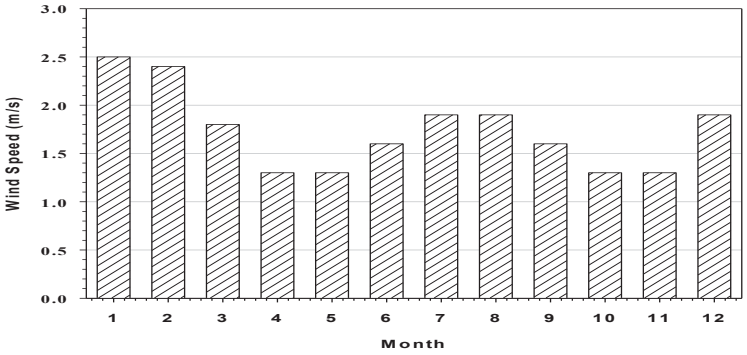

Fig. 7. Typical monthly wind speed in Singapore.

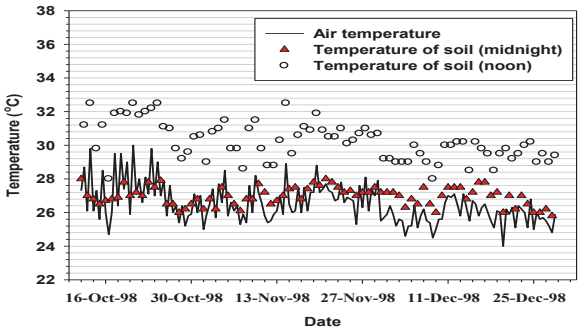

Fig. 8. Soil and air temperatures for residual soil slope at Yishun.

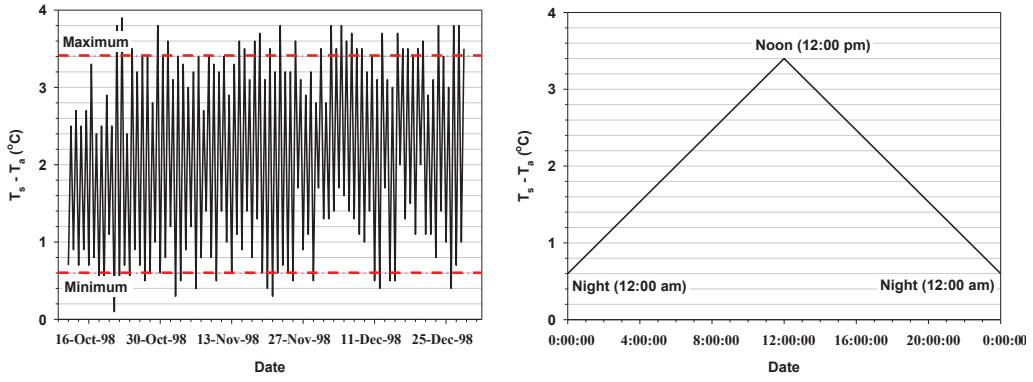

a. Actual daily variation

b. Typical variation in any given day

Fig. 9. Difference in soil and air temperatures for residual soil slope at Yishun.

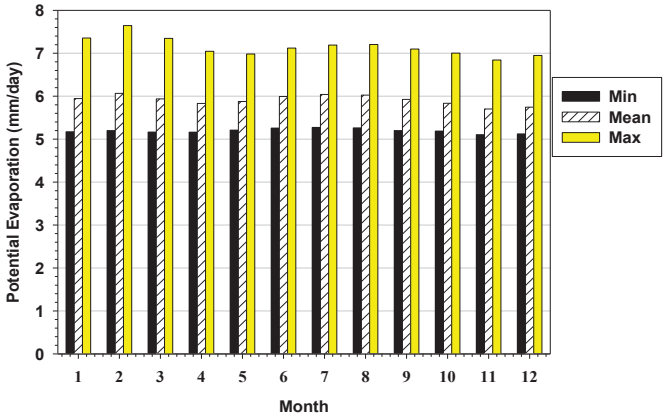

Fig. 10. Typical Potential Evaporation for Singapore calculated using Penman's equation.

4. Monitoring results of slope at Telok Blangah

Site instrumentation was carried out on a residual soil slope at Telok Blangah which is located at geological formation of Bukit Timah Granite (Fig. 11). Site investigations were performed to characterize properties of the soil as shown in Table 1. The soil-water characteristic curve (SWCC) data were obtained from laboratory tests using Tempe cell and pressure plate apparatuses. The permeability function of the soil was determined indirectly from SWCC using the statistical model[38,39,40] as explained in Fredlund and Rahardjo[11] and Fredlund et al.[12]. The SWCC and permeability function of the soil are shown in Figure 12 and Fig. 13. The SWCC variables of the soil are given in Table 2.

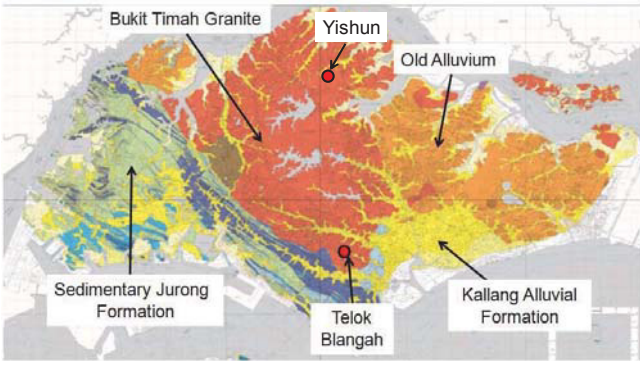

Fig. 11. Location of slope instrumentation in Singapore (modified from DSTA41).

The residual soil slope at Telok Blangah was instrumented with 6 tensiometers, 6 time-domain reflectometry (TDR), 6 soil temperature sensors, 2 piezometers and 1 set of weather station. Tensiometers, TDR and soil temperature sensors were installed in two rows at three different depths (0.5, 1.0 and 1.5 m). The real time instrumentation data could be extracted from the secured website and plotted with depth for a certain period of rainfall. The readings from weather station were used to plot the variation of air temperature, relative humidity and wind velocity with time (Fig. 14). The field instrumentation data were recorded every 5 minutes. The variations of rainfall and evaporation with time are shown in Fig. 15. The rainfall intensity was obtained from rain gauge reading whereas the potential evaporation rate was calculated from air temperature, relative humidity, solar net radiation and

wind velocity reading. The tensiometer and TDR readings were used to plot the pore-water pressure (Fig. 18) and volumetric water content (Fig. 19), respectively, within the instrumented site for a certain period of time.

Table 1. Properties of the residual soil at Telok Blangah

Properties	
Unified Soil Classification System	SC-CL
Specific gravity, G_s	2.46
Water content (%)	21.1
Gravel content (>4.75mm; %)	16.6
Sand (%)	30.5
Fines (<0.075mm; %)	52.9
Grain Size Distribution	
D_{60} (mm)	0.5
D_{30} (mm)	0.004
D_{10} (mm)	0.001
Dry density, ρ_d (Mg/m^3)	1.31
Liquid Limit, LL (%)	35
Plastic Limit. PL (%)	19
Saturated coefficient of permeability, k_s (m/s)	5.0×10^{-6}
Effective cohesion, c' (kPa)	3.3
Effective friction angle, ϕ' (°)	32

Table 2. SWCC variables of the residual soil at Telok Blangah

Variables	
Saturated volumetric water content, θ_s	0.46
Air-entry value, ψ_a (kPa)	1.14
Residual matric suction, ψ_r (kPa)	1500
Residual volumetric water content, θ_r	0.1
Fredlund and Xing fitting parameters	
a (kPa)	1.71
n	2.02
m	1.02

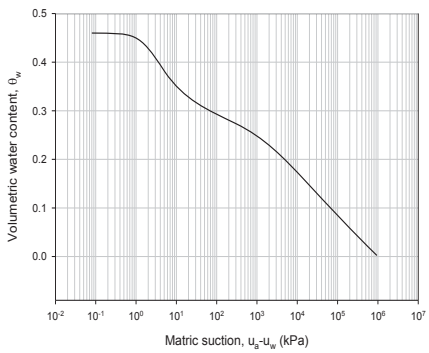

Figure 12. SWCC of the residual soil at Telok Blangah.

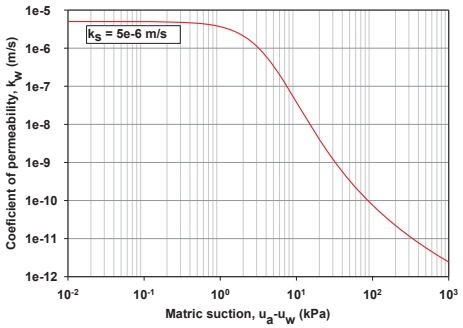

Fig. 13. Permeability function of the residual soil at Telok Blangah.

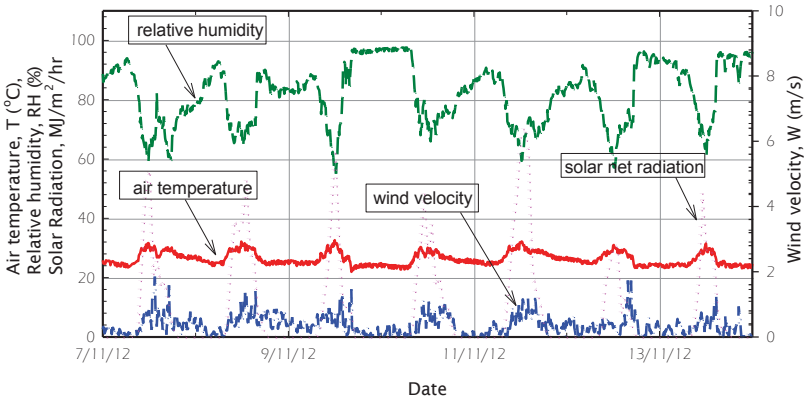

Fig. 14. Hourly variation of temperature, relative humidity, solar radiation and wind velocity at Telok Blangah site from 7 November to 13 November 2012.

Fig. 14 indicates that the mean air temperature of the residual soil at Telok Blangah from 7 November to 13 November 2012 was 27oC, similar to the typical mean air temperature in Singapore (Fig. 5). The range of relative humidity at Telok Blangah was between 60 to 90% which was in agreement with the typical relative humidity in Singapore (Fig. 6). The wind velocity at Telok Blangah is also in agreement with the typical wind velocity in Singapore (Fig. 7).

Fig. 15 indicates that the maximum rainfall and evaporation rates at Telok Blangah between 7 November and 13 November 2012 were 7.2 mm/hr and 1.2 mm/hr, respectively. The daily potential evaporation rate varies between 4 to 8 mm/day (Fig. 16), which is similar to the typical daily potential evaporation rate in Singapore (Fig. 10). However, the range at this site is wider. The daily potential evaporation rate range at Telok Blangah is between 4 to 8 mm/day while the typical range in Singapore is 5 to 7 mm/day. The fluctuation of potential evaporation rate is in agreement with the fluctuation of the solar net radiation (Fig. 14). As the solar net radiation increases, the potential evaporation rate also increases and vice versa. The daily actual evaporation rate calculated using the Wilson et. al.[36] equation shows very similar values as the daily potential evaporation rate because of the low suction on the ground surface corresponding to a high ground water table. The variation of soil temperature of the residual soil at Telok Blangah is illustrated in Fig. 17, indicating that the soil temperature variation near the ground surface was more noticeable than those at deeper depths. In addition, the variation of soil temperature at Telok Blangah was not as significant as the variation observed at Yishun and Mandai[32]. The difference could be attributed to the fact that the

soil temperature sensors at Telok Blangah (between 0.5 m and 1.5 m depths) were installed at deeper depths as compared to those sensors at Yishun and Mandai (between 0.05 m and 0.2 m depths). However, the trend of soil temperature variations at Telok Blangah was similar to those observed at Yishun and Mandai. The soil temperatures at Telok Blangah, Mandai and Yishun were high at noon and low at night.

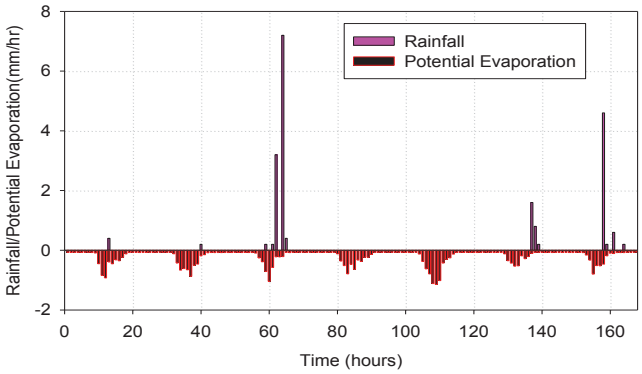

Fig. 15. Hourly variation of rainfall and potential evaporation rate of the residual soil at Telok Blangah from 7 November to 13 November 2012.

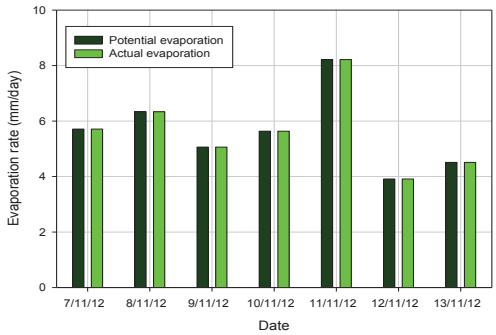

Fig. 16. Daily potential and actual evaporation rates of the residual soil at Telok Blangah from 7 November to 13 November 2012.

Fig. 18 shows that the pore-water pressure (PWP) at all depths increased significantly during rainfall due to water infiltration. When the rain stopped, the pore-water pressure decreased again since water had infiltrated into deeper depths. In addition, during dry period water moved upward due to evaporation near the ground surface. A similar trend was also observed in the variation of volumetric water content during dry and rainy periods. Fig. 19 indicates that the volumetric water content (VWC) changed significantly during rainfall and remained constant during dry period.

5. Seepage analyses of slope at Telok Blangah

Transient seepage analyses of two cases were carried out on the residual soil at Telok Blangah slope using the finite element software, SvFlux[42]. A 1-D model was used for the study in order to represent the exact location of the instrumentation. SvFlux software features a dynamic meshing algorithm which optimizes the mesh design. In this model, 201 nodes were used. There is no change in the number of nodes during the model run. The SWCC and permeability function of the soil were incorporated into the seepage analyses (Figure 12 and Fig. 13). The numerical

model for the finite element analysis was one-dimensional with a groundwater table at 0.96 m below the ground surface (Fig. 20). The field instrumentation data from one week monitoring period were selected for seepage analyses to investigate the characteristics of pore-water pressures within soil layers during dry and rainy periods. In this paper, the monitoring data from the month of November were selected since heavy rainfalls were observed during this period. In the first case (case 1), a natural rainfall was applied to the numerical model with the assumption of no evaporation occurring during the period of analysis. The rainfall data were taken from the rain gauge at the Telok Blangah site. In the second case (case 2), the potential evaporation and the natural rainfall were applied together in the analyses. The potential evaporation was applied in the analyses during dry and rainy periods. The potential evaporation rate was calculated based on Penman[37] equation with the input data coming from the instrumentation readings collected from the Telok Blangah site starting from 7 up to 13 November 2012. SvFlux could calculate the actual evaporation in several different ways. In this study, Wilson et.al.[36] equation was used in an uncoupled manner. This was done by assuming a constant soil temperature during the entire duration of the simulation. The temperature of the soil was assumed to be similar to the air temperature. The boundary condition at the top of the model was set as a unit flux equal to the specified rainfall and evaporation whereas the boundary condition at the bottom of the model was set as no flow boundary (Fig. 20).

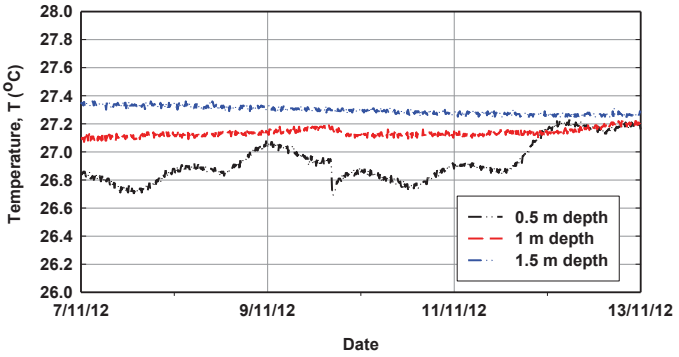

Fig. 17. Hourly variation of soil temperature at different depths for the residual soil at Telok Blangah from 7 November to 13 November 2012.

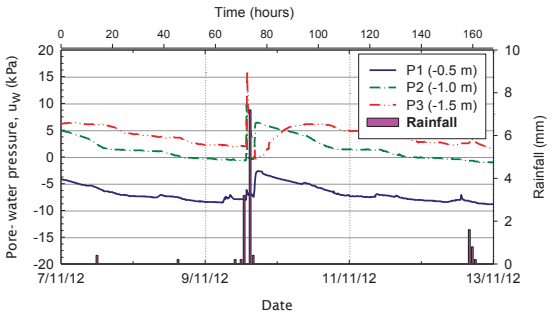

Fig. 18. Hourly variation of pore-water pressures obtained from tensiometer readings of the residual soil at Telok Blangah from 7 November to 13 November 2012.

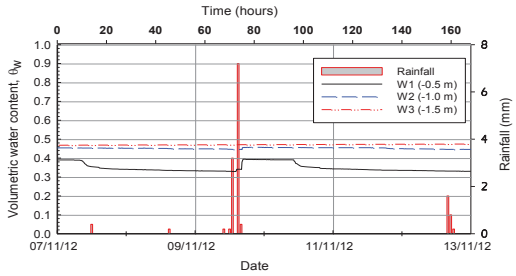

Fig. 19. Hourly variation of volumetric water content obtained from instrumentation readings of residual soil slope at Telok Blangah from 7 November to 13 November 2012.

The evaporation was adopted in the numerical analyses (case 2) to consider the effect of evaporation rate on the pore-water pressure and volumetric water content distributions in the residual soil at Telok Blangah. The results of cases 1 and 2 were compared with the data from the manual monitoring of tensiometer and TDR in the investigated site. The calculated actual evaporation rates have very similar values with the actual evaporation rates calculated using the numerical modeling as shown in Fig. 21. In the calculation, the soil temperature values obtained from the field measurements were input into the equation whereas in the numerical modeling the soil temperature values were assumed to be equal to the air temperature values. The very close values indicate that the difference between soil and air temperatures as used in the calculation does not give a significant effect in the calculated actual evaporation rate.

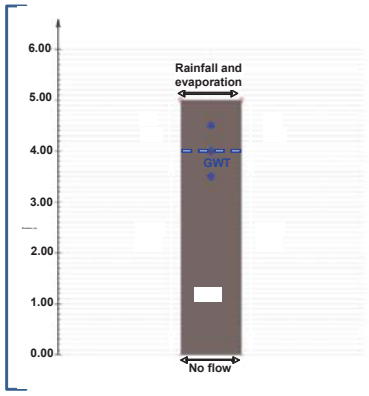

Fig. 20. 1-D numerical model for seepage analyses of the residual soil at Telok Blangah.

The pore-water pressure (PWP) distributions at different depths obtained from numerical analyses and instrumentation readings for case 1 for the period from 7 Nov to 13 Nov 2012 are shown in Fig. 22. During rainfall, the PWP obtained from the numerical analysis without evaporation increased and then became constant until the next rainfall occurred whereas the data showed an increase in PWP during rainfall and a decrease in PWP during drying. Therefore, In general, the pore-water pressure patterns from the numerical analyses did not show a good agreement with those obtained from tensiometer readings. The volumetric water contents (VWC) from the numerical analyses and instrumentation readings of case 1 are shown in Fig. 23. In general, the VWC trends from the numerical analyses were consistent with those from the instrumentation readings. The VWC values of the 1.0 and 1.5 m were very close because they were below the ground water table. However, the VWC values at depth 0.5 m were different from the measurement data The increase in VWC from the data was higher as compared to that from

the numerical modeling. The difference could be associated with the poor contact between the TDR and the soils in the investigated site since the soils contain a lot of granular materials (sand and gravel).

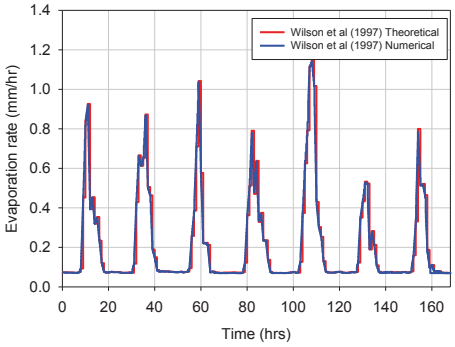

Fig. 21. Hourly variation of actual evaporation from calculation and from numerical modeling (7 November to 13 November 2012).

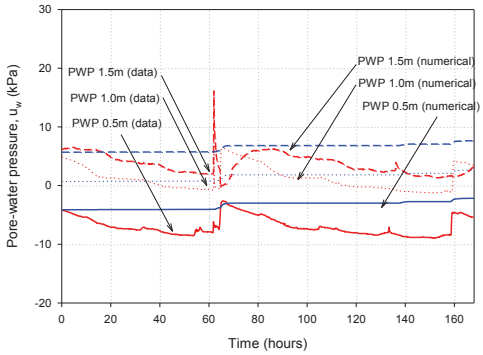

Fig. 22. Hourly variation of pore-water pressures obtained from tensiometer readings and results of case 1 seepage analyses (without evaporation).

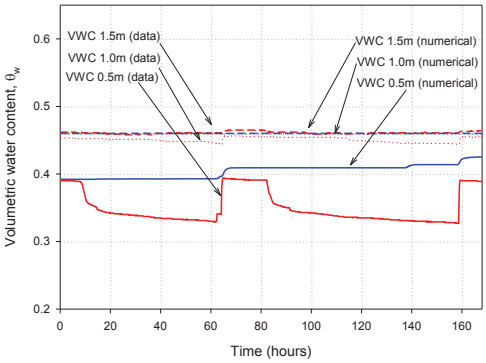

Fig. 23. Hourly variation of volumetric water contents obtained from instrumentation readings and results of case 1 seepage analyses.

The PWP and VWC distributions at different depths obtained from the instrumentation readings and results of seepage analyses for case 2 are shown in Fig. 24 and Fig. 25. During rainfall, the PWP increased significantly, showing the effect of rainfall on pore-water pressures at all depths. The VWC distributions also show a similar trend as compared to the instrumentation readings. However, similar to case 1, the VWC values differ significantly than those obtained from the numerical analyses. In general, the PWP patterns from the numerical analyses for case 2 showed a better agreement with those obtained from the tensiometer readings when compared with the results from the numerical analyses for case 1.

The comparison of PWP distributions obtained from the numerical analyses and instrumentation readings can be inspected further using the PWP profiles presented in Fig. 26 and Fig. 27 for case 1 and case 2, respectively. It can be seen that the numerical model with evaporation (case 2) fit the instrumentation data better than the model without evaporation (case 1). The better fit for the shallowest tensiometer was noticeable. After rainfall, the evaporation shifted the PWP line to more negative values, closer to the instrumentation data. Fig. 28 and Fig. 29 show the VWC profiles for case 1 and case 2, respectively. Similar to the PWP profiles, the VWC profiles for case 2 fit the instrumentation data better as compared to the VWC profiles for case 1. Both the PWP and VWC profiles at the shallowest depth during drying condition always showed drier condition than those obtained from the seepage modeling. This could be caused by the effect of transpiration that was not taken into account in the seepage modeling. Another cause might be due to the low accuracy of SWCC and permeability function.

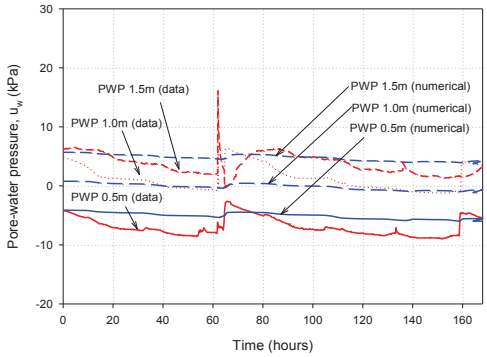

Fig. 24. Hourly variation of pore-water pressures obtained from tensiometer readings and case 2 seepage analyses (with evaporation).

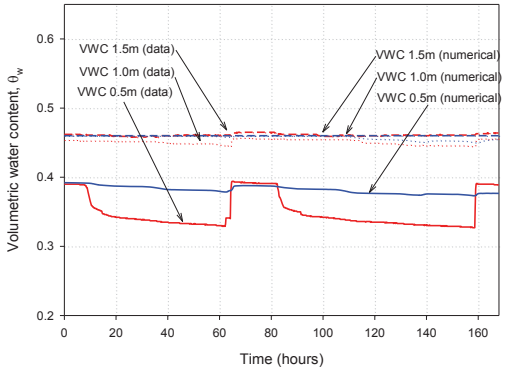

Fig. 25. Hourly variation of volumetric water contents obtained from instrumentation readings and case 2 seepage analyses (with evaporation).

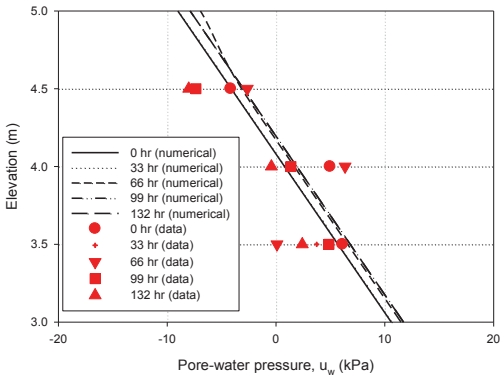

Fig. 26. Pore-water pressure profiles obtained from tensiometer readings and seepage analyses for Case 1 (without evaporation).

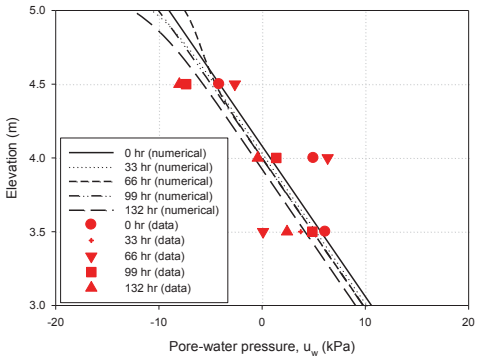

Fig. 27. Pore-water pressure profiles obtained from tensiometer readings and seepage analyses for Case 2 (with evaporation).

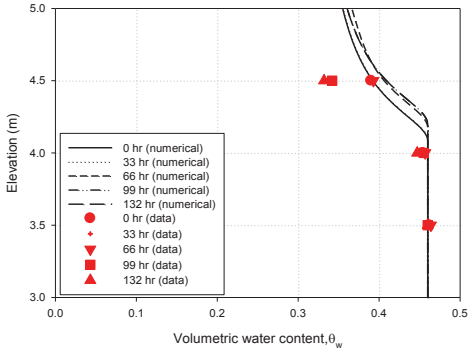

Fig. 28. Volumetric water content profiles obtained from tensiometer readings and seepage analyses for Case 1 (without evaporation).

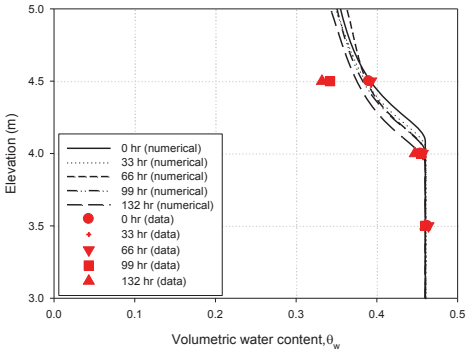

Fig. 29. Volumetric water content profiles obtained from tensiometer readings and seepage analyses for Case 2 (with evaporation).

6. Parametric studies

Parametric studies were carried out to observe the role of soil-water characteristic curve (SWCC) and coefficient of saturated permeability in affecting the pore-water pressure distribution and volumetric water content during dry and rainy periods. Two cases of numerical analyses were conducted in these parametric studies. In the first seepage analysis (case 3), the soil was assumed of having a lower permeability than the soil used in the seepage analysis as described in Section 4. In the second seepage analysis (case 4), the soil was assumed to have SWCC with a higher air-entry value than the soil used in the seepage analysis as described in Section 4. Similar boundary conditions, rainfall intensity and evaporation rate were applied in the numerical analyses of the parametric studies.

6.1. Soil with low permeability

In case 3 (the first seepage analysis of the parametric study), the saturated permeability of the soil was assumed to be 5×10^{-8} m/s, lower than that used in cases 1 and 2 (i.e., 5×10^{-6} m/s) The SWCC of the soil was assumed the same as that used in cases 1 and 2 (Figure 12). The permeability function of the soil for case 3 was calculated using the assumed value of coefficient of saturated permeability of 5×10^{-8} m/s and the SWCC given in Fig. 12. The PWP and VWC distributions from case 3 are shown in Fig. 30 and Fig. 31. It can be seen that the pore-water pressure from the seepage analysis of case 3 did not show any changes during dry and rainy periods due to the low coefficient of saturated permeability of the soil. As a result, water infiltrated the soil in a very slow rate, causing no change in the PWP. Similarly, the volumetric water contents from the numerical analyses of case 3 (Fig. 31) appeared as horizontal lines, indicating that the VWCs of the soil were not affected by the rainfall and evaporation processes. These numerical results did not agree with the measurement data. Therefore, the accuracy of coefficient of saturated permeability is critical in the numerical modeling of flux boundary conditions.

6.2. Soil with high air-entry value

In case 4 (the second seepage analysis of the parametric study), the air-entry value of the SWCC was assumed to be 3.7 kPa, higher than that used in cases 1 and 2 (1.2 kPa). The coefficient of saturated permeability of the soil was assumed to be the same as that used in cases 1 and 2 (i.e., 5×10^{-6} m/s). The permeability function of the soil for case 4 was calculated using the assumed air-entry value of 3.7 kPa and the original coefficient of saturated permeability (i.e., 5×10^{-6} m/s). The PWP and VWC distributions from case 4 are shown in Fig. 32 and Fig. 33. The PWP and VWC profiles from case 4 are shown in Fig. 34 and Fig. 35. The PWP profile followed the trend of the instrumentation reading very well. During drying process, the PWP in case 4 (Fig. 32) decreased in a steeper slope as compared to that of case 2 (Fig. 24) which followed the instrumentation data very well. Therefore, during rainfall the match between PWP of case 4 and the instrumentation data is better than between case 2 and the instrumentation

data. The changes in air-entry value or the SWCC parameters affected the permeability function of the material. By having a higher air-entry value, the soil usually has a higher permeability for a given suction. This higher permeability might be the cause of the better fit with the instrumentation data during drying process of case 4.

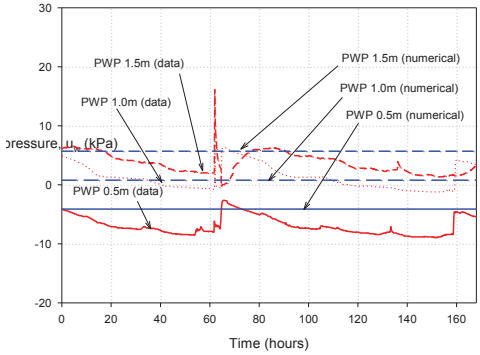

Fig. 30. Hourly variation of pore-water pressures obtained from tensiometer readings and seepage analyses for case 3 (using soil with a low coefficient of saturated permeability; ks = 5 × 10-8 m/s).

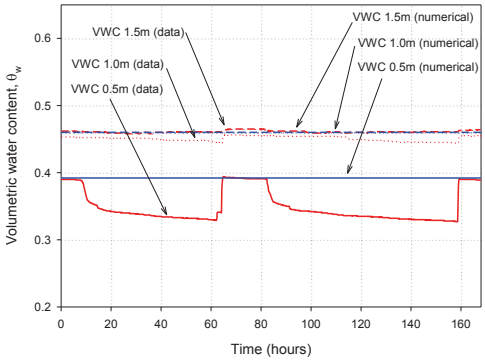

Fig. 31. Hourly variation of volumetric water contents obtained from intrumentation readings and seepage analyses for case 3 (using soil with a low coefficient of saturated permeability; ks = 5 x 10-8 m/s).

6.3. Discussion of parametric studies

The results of parametric studies indicated that soil properties affected the pore-water pressure (PWP) and volumetric water content (VWC) greatly during infiltration and evaporation. SWCC and permeability function are critical parameters for an appropriate seepage modelling. The monitoring data from field instrumentation will not be in agreement with the results from the seepage modelling without proper measurements of SWCC and permeability function. The numerical model used in this study focused on the effect of flux boundary on PWP and VWC in 1-D condition. Factors that affect the seepage analysis in 3-D conditions such as the steepness of the slope and drainage conditions around the studied area were not taken into account in this study.

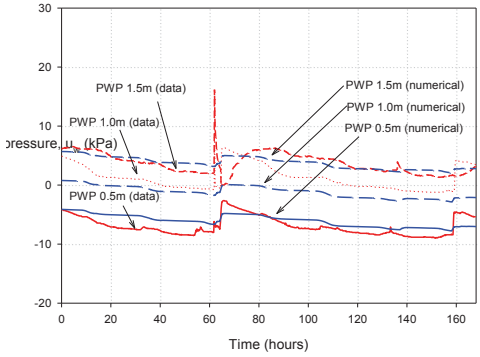

Fig. 32. Hourly variation of pore-water pressures obtained from tensiometer readings and seepage analyses for case 4 (using soil properties with a high air-entry value; AEV = 3.70 kPa).

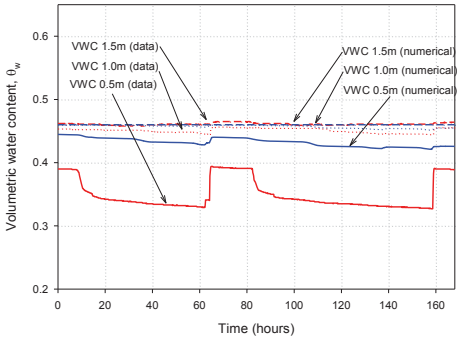

Fig. 33. Hourly variation of volumetric water contents obtained from intrumentation reading and seepage analyses for case 4 (using soil properties with a high air-entry value; AEV = 3.70 kPa).

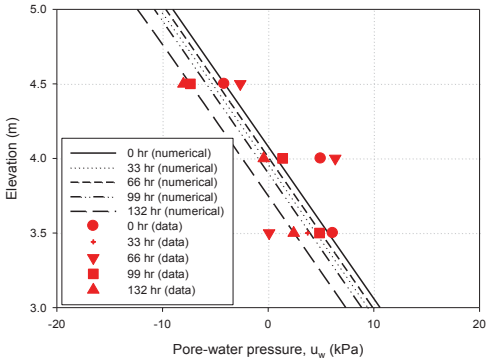

Fig. 34. Pore-water pressure profiles obtained from tensiometer readings and seepage analyses for Case 4 (using soil properties with a high air-entry value; AEV = 3.70 kPa).

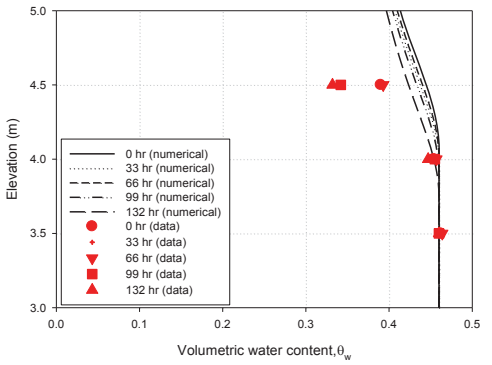

Fig. 35. Volumetric water content profiles obtained from tensiometer readings and seepage analyses for Case 4 (using soil properties with a high air-entry value; AEV = 3.70 kPa).

7. Conclusions

The characterization of climatic data is necessary for quantifying flux boundary conditions. Variation of pore-water pressure and volumetric water content during dry and rainy periods can be assessed realistically using principles of unsaturated soil mechanics in characterizing unsaturated soil properties (i.e., soil-water characteristic curve and permeability function) and seepage analyses as well as measurements of negative pore-water pressures, soil moisture and soil temperature. Different types of instruments can be used to observe the variation of pore-water pressure and volumetric water content in a residual soil slope during rainfall and evaporation in real time. The pore-water pressure profiles from seepage analyses in 1-D condition showed a reasonably good agreement with those obtained from field measurements if actual evaporation was incorporated in the seepage analyses. The results from the parametric studies indicated that proper measurements of soil properties (SWCC and permeability function) are very important in order to obtain appropriate simulations of pore-water pressure distributions within the soil.

Acknowledgements

The authors would like to acknowledge the assistance provided for this study by Geotechnics Laboratory staff, School of Civil and Environmental Engineering, Nanyang Technological University, Singapore.

References

1. Malone AW. Risk Management and Slope Safety in Hongkong. *Transactions of The Hongkong Institution of Engineers* 1997;**4(2-3)**:1-90.
2. Derbyshire E. *Geomorphology and Climate*. London: John Wiley; 1976.
3. Toll DG, Rahardjo H, Leong EC. Landslides in Singapore. In: *Proc. 2nd International Conference on Landslides, Slope Stability and the Safety of Infra-Structures*, Singapore: 1999; p. 269-276.
4. Fukuoka M. Landslides Associated with Rainfall. *Geotechnical Eng* 1980;**11**:1-29.
5. Campbell RH. *Soil Slips, Debris Flows, and Rainstorms in Santa Monica Mountains and Vicinity, Southern California*. US Geological Survey; 1975.
6. Bennett MR, Doyle P. *Geology and The Human Environment. Environmental Geology*. 1997. Chichester, John Wiley & Sons Ltd.
7. Rahardjo H, Satyanaga A, Leong EC. Slope Failures in Singapore due to Rainfall. In: *Proc. Australia New Zealand Conference on Geomechanics "Common Ground"*. Brisbane, Australia 2007; p. 704-709.
8. Sower GF. Natural Landslides. In: *Proc. ASCE Geotechnical Engineering Specialty Conference on Stability and Performance of Slopes and Embankments – II*, Berkley, California. 1992, p. 804-833.
9. Broms BB, Wong KS. Landslides. In: *Foundation Engineering Handbook*, VanNorstand Reinhold, New York. 1991; p. 410-446.
10. Brand EW. State-Of-The-Art Report of Landslides in Southeast Asian, In: *Proc. 4th International Symposium on Landslides,* Toronto, Canada. 1984; p. 17-37.
11. Fredlund DG, Rahardjo H. *Soil Mechanics for Unsaturated Soils*, John Wiley & Sons, New York; 1993.
12. Fredlund DG, Rahardjo H, Fredlund MD. *Unsaturated Soil Mechanics in Engineering Practice*. John Wiley & Sons, Inc., New York; 2012.

13. Wilson GW, Machibroda RT, Barbour LS, Woyshner MR. Modelling of Soil Evaporation from Waste Disposal Sites. In: *Proc. 1993 Joint CSCE-ASCE National Conference on Environmental Engineering*, 1993; p. 281-288.
14. Gasmo J, Hritzuk KJ, Rahardjo H, Leong EC. Instrumentation of an Unsaturated Residual Soil Slope. *Geotech Test J* 1999;**22(2)**:128-137.
15. Springman SM, Teysserie P. Artificially induced rainfall instabilities on moraine slopes. In: Kuhne M et al., editors. *Proc. International Conference on Landslides*, Davos, VGE, Essen; 2001; p. 209-223.
16. Gitirana Jr G, Fredlund DG, Fredlund MD. Infiltration-runoff boundary conditions in seepage analysis. In: *Proc. 58th Canadian Geotechnical Conference,* Saskatoon, Canada*:* 2005; p. 516-523.
17. Kilsby C, Glendinning S, Hughes PN, Parkin G, Bransby MF. Climate-change impacts on long-term performance of slopes. *Proceedings of the Institution of Civil Engineers, Engineering Sustainability* 2009;**162(ES2)**:59-66.
18. Rouainia M, Davies O, O'Brien T, Glendinning S. Numerical modeling of climate effects on slope stability. *Proceedings of the Institution of Civil Engineers, Engineering Sustainability* 2009;**162(ES2)**:81-89.
19. Mendes J. *Assessment of the impact of climate change on an instrumented embankment: an unsaturated soil mechanics approach*. Doctoral thesis, 2011, Durham University.
20. Glendinning S, Loveridge F, Starr-Keddle RE, Bransby MF, Hughes PN. Role of vegetation in sustainability of infrastructure slopes. *Proceedings of the Institution of Civil Engineers, Engineering Sustainability* 2009;**162(ES2)**:101-110.
21. Springman SM, Jommi C, Teysserie P. Instabilities on moraine slopes induced by loss of suction: a case history. *Geotechnique* 2003;**53(1)**:3-10.
22. Jotisankasa A, Vathananukij H, Coop MR. Soil-Water Retention Curves of Some Silty Soils and Their Relations to Fabrics. In: *Proc. The 4th Asia Pacific Conference on Unsaturated Soils*, Newcastle, Australia: 2009; p. 263-268.
23. Johnson KA, Sitar N. Hydrologic conditions leading to debris-flow initiation. *Canad Geotech J* 1990;**27**:789-801.
24. Cascini L, Cuomo S, Pastor M, Fernandex-Merodo JA. Groundwater modelling of a weathered gneissic cover. *Canad Geotech J* 2006:**43**:1153-1166.
25. Evangelista A, Nicotera MV, Papa R, Urciuoli G. Field investigation on triggering mechanisms of fast landslides in unsaturated pyroclastic soils. In: *Proc. 1st European Conference on Unsaturated Soils*, Durham, UK. 2008; p. 909-915.
26. Alonso EE, Gens A, Delahaye CH. Influence of rainfall on the deformation and stability of a slope in overconsolidated clays: a case study. *Hydrogeol J* 2003;**11**:174-192.
27. Liew SS, Liong CH, Low CL. Four landslide investigations in Malaysia. In: *Proc. 15th SEAGC*, Bangkok, Thailand 2004.
28. Brand EW. Slope instability in tropical areas. In: *Proc. 6th International Symposium on Landslides*, Christchurch, New Zealand. 1992; p. 2031-2051.
29. Rahardjo H, Satyanaga A, Leong EC, Ng YS. Effects of groundwater table position and soil properties on stability of slope during rainfall. *ASCE J Geotech Geoenviron Eng* 2010;**136(11)**:1555-1564.
30. Rahardjo H, Lee TT, Leong EC, Rezaur RB. Response of a Residual Soil Slope to Rainfall. *Canad Geotech J* 2005;**42**:340-351.
31. Wilson GW. *Soil evaporative fluxes for geotechnical engineering problems*. PhD thesis, University of Saskatchewan, Saskatoon, Canada; 1990.
32. Rahardjo H, Satyanaga A, Leong EC. Effects of flux boundary condition on pore-water pressure distribution in slope. *Eng Geol* 2013;**165**:133-142.
33. Biomachine Pte Ltd. *Report of site monitoring for the assessment of the effect of rainfall and evaporation on landfill sustainability at Lorong Halus*. Singapore; 2013.
34. McGraw-Hill Companies, *Meteorology Source Book*; 1988.
35. National Environment Agency. *Meteorological Services Data*. Singapore; 2010
36. Wilson GW, Fredlund DG, Barbour SL. The Effect of Soil Suction on Evaporative Fluxes from Soil Surfaces. *Canad Geotech J* 1997;**34**:145-155.
37. Penman HL. Natural evapotranspiration from open water, bare soil and grass. *Proc. Royal Society of London Serial A* 1948;**193**:120-145.
38. Marshall TJ. A relation between permeability and size distribution of pores. *J Soil Sci* 1958;**9**:1-8.
39. Millington RJ, Quirk JP. Permeability of porous media. *Nature* 1959;**183**:387-388.
40. Kunze RJ, Uehara G, Graham K. Factors important in the calculation of hydraulic conductivity. *Proc Soil Sci Soc Am* 1968;**32**:760-765.
41. DSTA. *Geology of Singapore 1st Edition*, Singapore; 1976.
42. SoilVision Systems Ltd.,. *SVFlux user's manual*, version 2.4.09. Saskatoon, Saskatchewan; 2009.